Helium Bubble Kinetics during Laser Welding of Helium-Doped Stainless Steel†

Toshio KURODA*, Fukuhisa MATSUDA and Yasuyuki FUJIYA*****

Abstract

Helium is generated within neutron-irradiated reactor components and entrapped in the stainless steel components. The repair of the components using conventional GTA welding practices is then exceedingly difficult, because of the creation of helium bubbles and weld cracking.

In this research, the behavior of helium bubbles in austenitic stainless steel weldments was investigated using stainless steel helium ion-implanted and then welded using YAG Laser apparatus. Helium ion implanting of the sample was carried out using 8MeV implantation apparatus, the sample being doped $2.45x10^{19}/m^2$ at 6MeV and then doped $1x\ 10^{19}/m^2$ at 5MeV.

Helium bubbles are present at the bond region, heat-affected zone and weld metal. An increase of weld heat input causes the growth of helium bubbles and produce toe cracks and cracks along the dendrite cell boundary in the weld metal. The helium bubble phenomena can be simulated in the weld metal and in the heat-affected zone during repair welding using helium ion implanting technique.

Keywords: (Helium Bubble) (Helium Ion Implanting) (Austenitic Stainless Steel) (Toe Cracking) (Dendrite Cell) (Weld Metal) (HAZ)

1. Introduction

Nuclear reactors at the Savannah River Plant built in the early 1950's produced radioactive materials but no electricity was generated. One of the five reactors has a curve knuckle transition piece joining the tank sidewall to the bottom. This region was sensitized during tank fabrication and developed stress corrosion cracking during service[1].

The cracks resulted in leaks that were first repaired in 1968 using GTA welding. The tank leaked again in 1984. Weld toe cracking on the irradiated wall of a nuclear reactor tank was then observed. Consequently the repair of the reactor tank using conventional GTA welding practices is made exceedingly difficult, because of entrapped helium[2)-4)].

The helium is formed by neutron reactions with alloy constituents, principally with boron, as

$$^{10}B + n \longrightarrow {}^{7}Li + {}^{4}He$$

and with nickel as

$$^{58}Ni + n \longrightarrow {}^{59}Ni + \gamma,$$

$$^{59}Ni + n \longrightarrow {}^{56}Fe + {}^{4}He.$$

The very low solubility of helium in steels results in its tendency to form small bubbles.

Preferred nucleation sites for these helium bubbles are radiation-induced lattice defects, precipitate interfaces, dislocations and grain boundaries.

At elevated temperatures, these bubbles grow very rapidly and under applied stress, can severely weaken the boundaries. Welding processes produce internal stresses and elevated temperatures which may enhance the growth rate of helium bubbles and accelerate the degradation of properties.

In case of GTA welding, toe cracking and under bead cracking were observed, which showed an intergranular fracture form related to helium bubbles[2),3)].A quantitative understanding of the relationship between helium and weld cracking has not been developed.

In order to implant helium into the test material, the tritium trick technique was employed. In this technique, tritium gas is diffused into the material at elevated temperatures. The dissolved tritium is then allowed to decay to form helium by the reaction. $^{3}H \rightarrow \beta^{-} + {}^{3}He$ with a half-life of 12.3 years.

Two techniques were developed. First[3)], all samples were charged at 300℃ with tritium pressure ranging from 0.07 to 125Mpa for 30 days. After that, the samples were degased at 400°C in a vacuum of 10^{-3}Pa to remove

† Received on July 21, 1995
* Assistant Professor
** Professor
*** Mitsubishi Heavy Industries, Ltd

Transactions of JWRI is published by Welding Research Institute of Osaka University, Ibaraki, Osaka 567, Japan.

residual tritium.

In the second method[2], all the samples were held at 400°C for 30 days in tritium gas. After which samples were vacuum degassed at 450°C for 5 days.

Recently, high energy 8MeV ion implanting apparatus has been developed. In this investigation, helium ions were implanted into stainless steel using this apparatus, and then the samples were laser-welded. The relation between helium bubble phenomena and welding condition was investigated.

2. Experimental Procedure.

The material used in this investigation is SUS316L stainless steel with 0.5 mm thickness and the chemical composition is shown in **Table 1**. Helium ion implanting was carried out using 8MeV ion implanting apparatus[5] shown in **Fig.1**.

The conditions of helium ion implanting of the sample are shown in **Table 2**. The temperature of the samples after the implantation was measured, and heated up to 317K.

After implantation, bead on plate welding was carried out using a YAG Laser apparatus as shown in **Fig.2**.

The welding condition is shown in **Table 3**. The behavior of helium bubbles was observed in detail using the Scanning Electron Microscope.

Table 1 Chemical composition of SUS316L stainless steel (mass%)

Material	C	Si	Mn	P	S	Ni	Cr	Mo	Cu
SUS316L	0.030	0.75	0.97	0.019	0.009	12.07	17.30	2.22	0.24

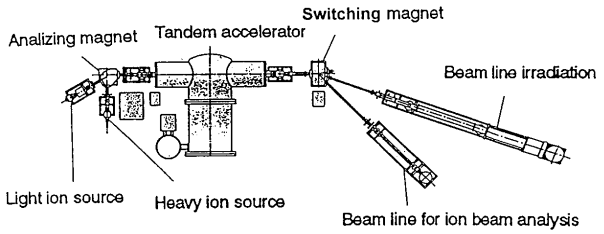

Fig.1 Schematic illustration of 8MeV ion implanter

Table 2 Condition of helium ion implanting

Ion	Accelerated voltage (MeV)	Implanted dose (atoms/m^2)	Temperature (K)	Time (ks)
He^{2+}	6	2.45 x10^{19}	317	54
He^{2+}	5	1.00 x10^{19}	317	54

Table 3 Welding condition after helium implanting

Sample No.	1	2	3	4	5	6	7	8	9	10	11	12
Laser power (W)	40	50	70	90	80	100	140	180	160	200	280	360
Travel speed(m/s)	1.3 x10^{-2}				3.3x10^{-2}				1.3x10^{-1}			

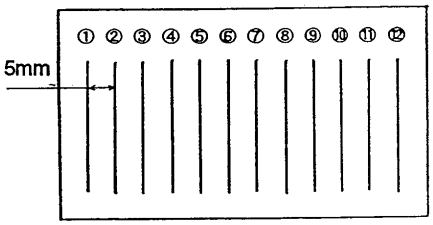

Fig.2 Schematic presentation of sample welded by YAG laser apparatus

3. Results

3.1 Depth profiles of helium atoms

Numerical calculation of helium distribution was made using the Monte Carlo simulation technique (TRIM 95)[6], as 10000 helium atoms were implanted at 5MeV and at 6MeV. The results are shown in **Fig.3**. Channeling effects were ignored.

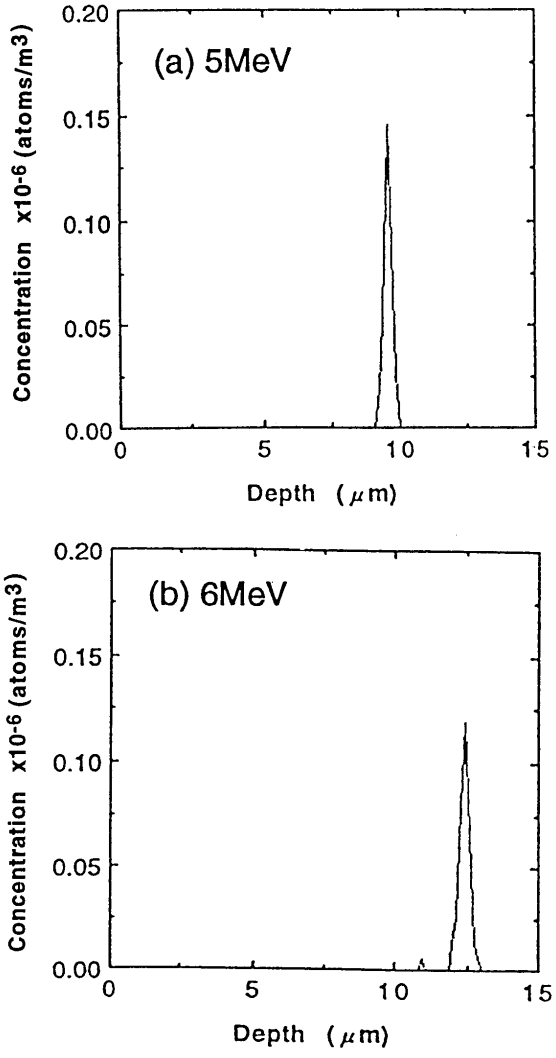

Fig.3 Distribution of helium atoms by Monte Carlo Calculation (TRIM85)

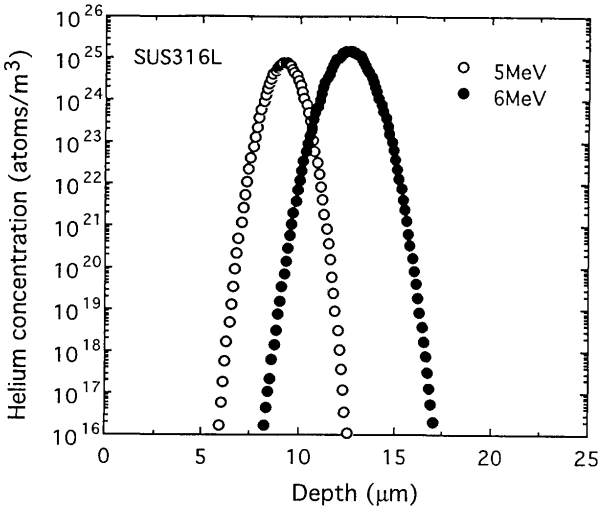

Fig.4 Depth profiles of 6MeV and 5MeV helium ion implants in SUS316L stainless steel

The depth of maximum dose from the sample surface is 12.5μm with 6MeV and 9.8μm with 5MeV. As the results, the samples were dosed at 2.45×10^{19} atoms/m^2 with 6MeV and dosed at 1×10^{19} atoms/m^2 with 5MeV.

According to the LSS (Lindhard Scharff and Schiott) theory[7], helium concentration F(X) is shown by a Gauss distribution curve described by equation (1).

$$F(X)=N/((\sqrt{2\pi})\Delta Xp)\exp\{-(X-Xp)^2/(2\Delta Xp^2)\} \quad \text{----(1)}$$

In case of 6MeV,

$N=2.45\times10^{19}$atoms/m^2, $\Delta Xp=6.8\times10^{-7}$m,

$Xp=1.256\times10^{-5}$m

In case of 5MeV,

$N=1\times10^{19}$atoms/m^2 ,$\Delta Xp=5.2\times10^{-7}$m,

$Xp=9.18\times10^{-6}$m

Figure 4 is obtained by specifying these values. SUS 316L stainless steel has 71at%Fe, 18at%Ni and 1at%Mo, and the average mass is 55.836.

The density is 8.03×10^6 g/m^3. The atomic number in the SUS316L steel is $6.02\times10^{23} \times 8.03 \times 10^6 / 55.836 = 8.66 \times10^{28}$ atoms/m^3.

Consequently, the maximum helium concentration is $1.43\times10^{25}/8.66\times10^{28}=165$ appm at 12.5μm from the surface with 6Mev and $7.67\times10^{24}/8.66\times10^{28}=88.5$ appm at 9.18μm from the surface with 5MeV.

3.2 Behavior of helium bubbles in the Laser weldments

Figure 5 shows the bead surface, after the helium-doped SUS316L steel was welded at a Laser power of 50W and a travel speed of 1.3×10^{-2} m/s. Large helium

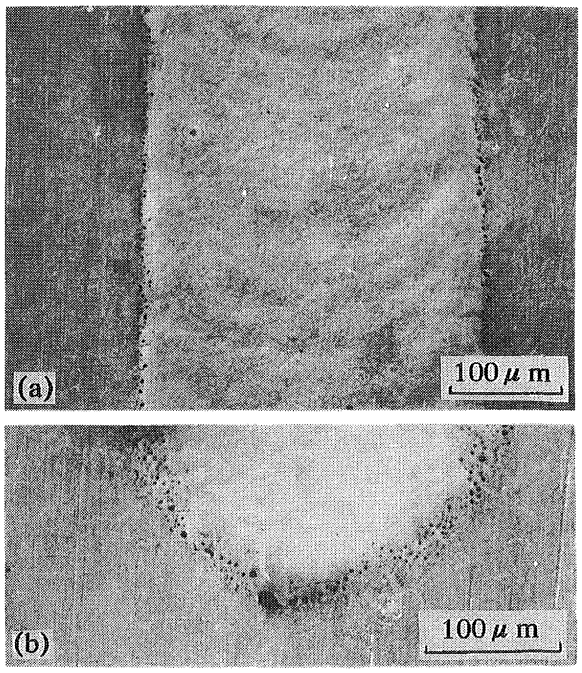

Fig.5 Surface appearances of YAG laser weld. Power 50W, Travel speed 1.3x10-2m/s, (a):Bead center area, (b):Bead start area

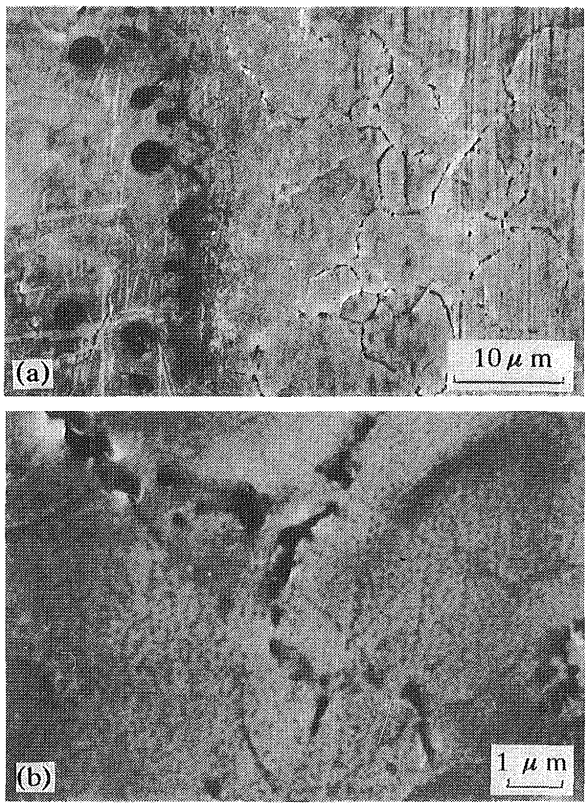

Fig.6 Surface appearnces of YAG laser weld. Power 50W, 1.3×10^{-2}m/s, (a):Bond region, (b):Heat-affected zone

bubbles were observed near the bond region between bead and heat affected zone in both the bead center area(a) and the bead start area(b).

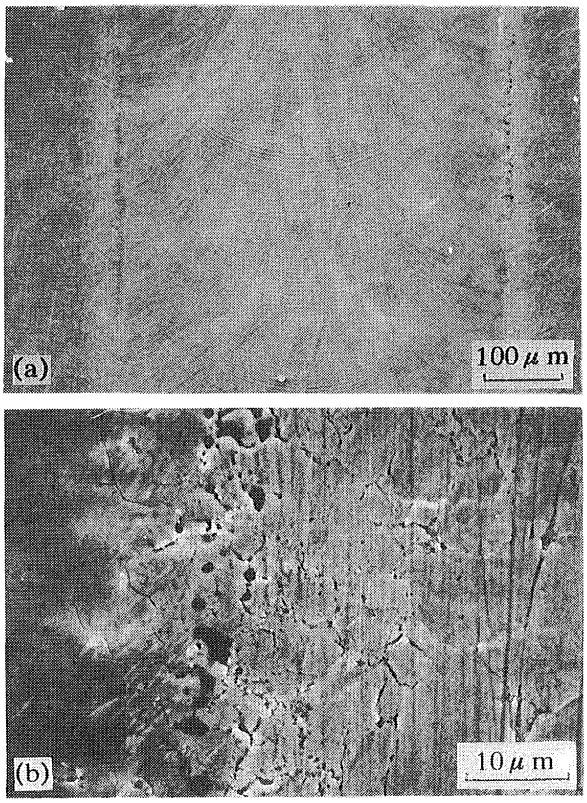

Fig.7 Surface appearances of YAG laser wels. Power 90W, $1.2x10^{-2}$m/s, (a):Bead center area, (b):Bond region

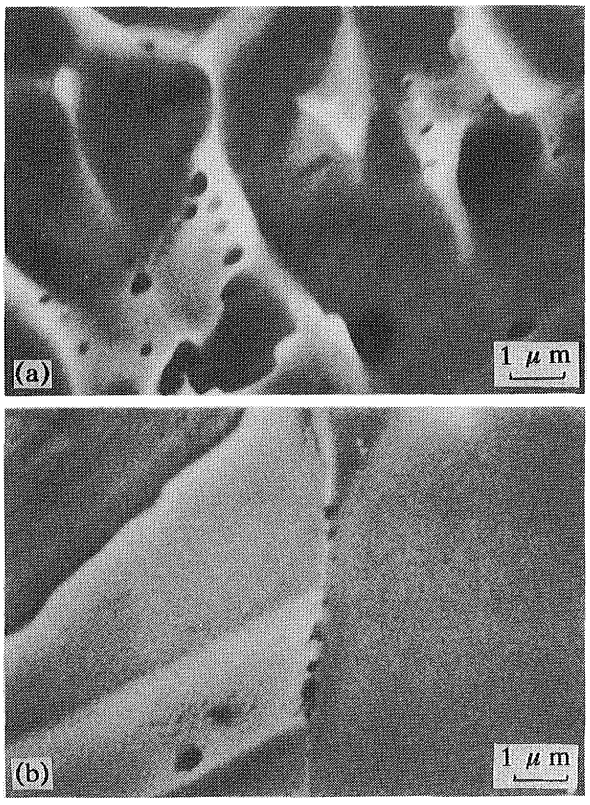

Fig.8 Cross sectional area of YAG laser weld. Power 90W, Travel speed $1.2x10^{-2}$m/s, (a):Weld metal, (b):Heat-affected zone

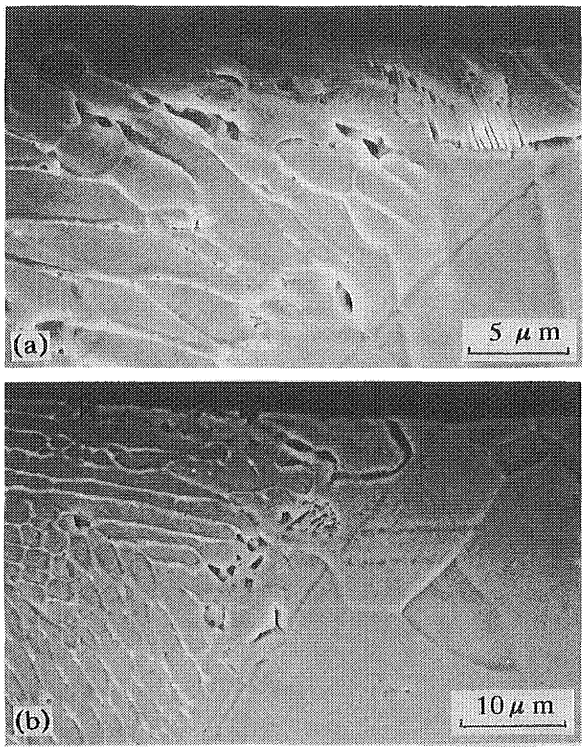

Fig.9 Cross sectional microstructures of YAG laser welds. (a):Power 140W, Travel speed $3.3x10^{-2}$m/s, (b):Power 180W, Travel speed $3.3x10^{-2}$m/s

This technique reproduces the helium bubble phenomenon during the real repair welding of the helium contaminated SUS316L steel.

Figure 6 is an enlargement of Fig.5. Large helium bubbles with 3 to 4 μm size are observed near the bond region between the bead and the heat affected zone. In particular, helium bubbles are continuously present at the grain boundaries in the heat affected zone.

Figure 6-(b) shows helium bubbles at the grain boundary. Such helium bubbles are rarely observed in the helium-doped SUS316L steel before welding.

Consequently, it is concluded that the helium bubbles are generated during laser welding.

Figure 7 indicates the bead surface after the helium doped SUS316L steel was welded at a laser power of 90W and a travel speed of $1.3x10^{-2}$m/s.

Helium bubbles are observed near the bond region between bead and heat affected zone. The number of large helium bubbles is less than appears in Fig.6.

Fine helium bubbles are discontinuously present at the heat affected zone. The bead width and volume increased with increasing weld heat input.

Figure 8 shows the cross sectional area of the welds, when the helium doped SUS316L stainless steel was welded using laser power of 90W and travel speed of $1.3x10^{-2}$m/s.

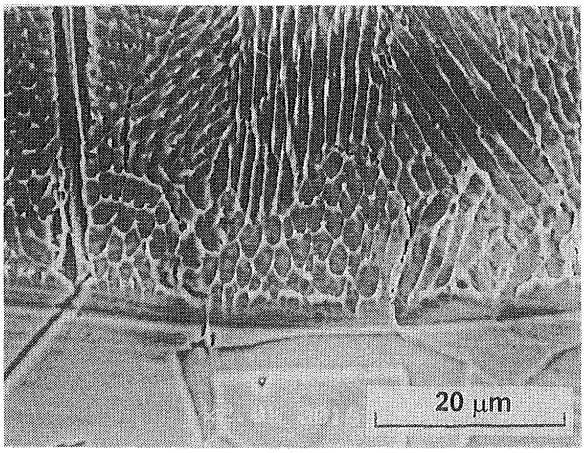

Fig.10 Cross sectional microstructure of YAG laser welds, Power 100W, $3.3x10^{-2}$m/s

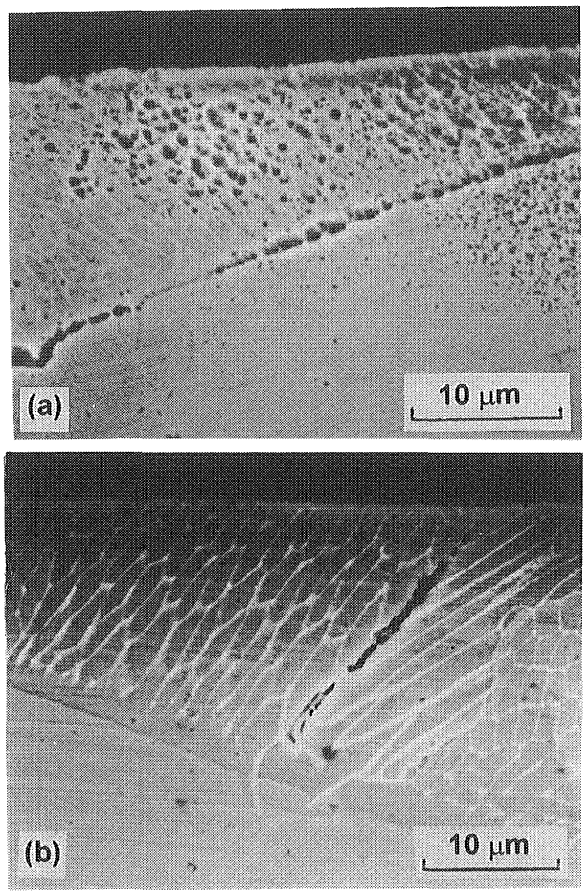

Fig.11 Cross sectional microstructures of YAG laser welds. Power 160W, Travel speed $1.3x10^{-1}$m/s

Helium bubbles of about 0.3μm diameter are observed at the dendrite cell boundary in the weld metal. Helium bubbles with diameter of 0.1 to 0.2μm are observed within the grain and at the grain boundary in the heat affected zone.

Figure 9 shows the cross sectional areas of the welds, when the helium-doped SUS316L steels were welded at a laser power of 140W(a) and 180W(b). These samples represented high weld heat input.

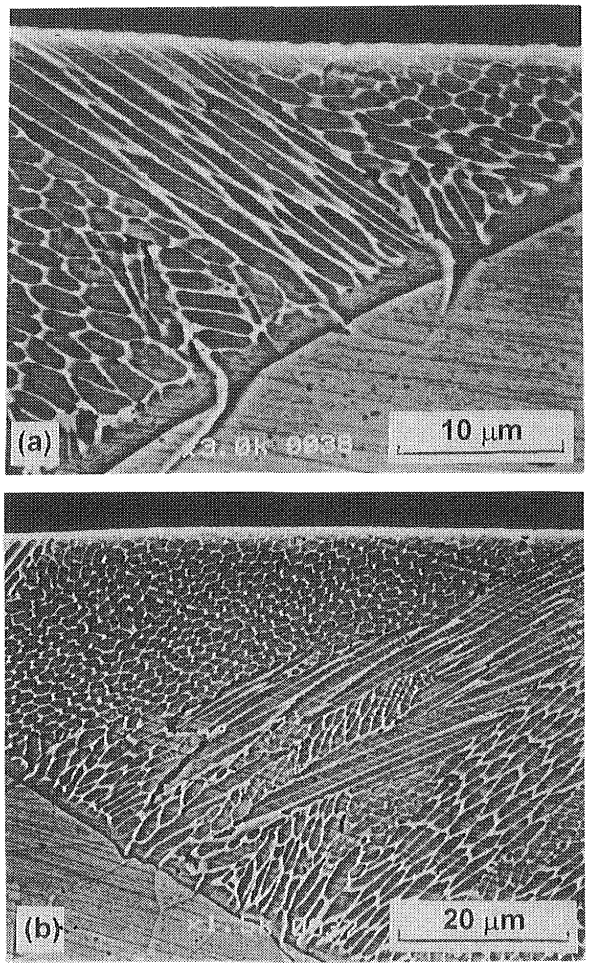

Fig.12 Cross sectional microstructures of YAG laser welds. Power 200W, Travel speed $1.3x10^{-1}$m/s

In case of a laser power of 140W, as shown in Fig.9-(a), cracks and helium bubbles are observed at the dendrite cell boundary. In case of Laser power of 180W, large helium bubbles are observed at the dendrite cell boundary and toe cracks occurred at the bond region related to the continuous helium bubbles.

Figure 10 shows the cross sectional area, when the helium doped SUS316L steel was laser welded. Helium bubbles are continuously present at the grain boundaries and the dendrite cell boundaries, and lead to the cracks in the weld metal.

Figure 11 shows the cross sectional area of YAG Laser welds, after the helium-doped SUS316L steel was welded at a laser power of 160W and travel speed of $1.3x10^{-1}$m/s.

A number of large helium bubbles are continuously present at the bond region and many helium bubbles are present in the weld metal and in the heat affected zone as shown in Fig.11-(a).

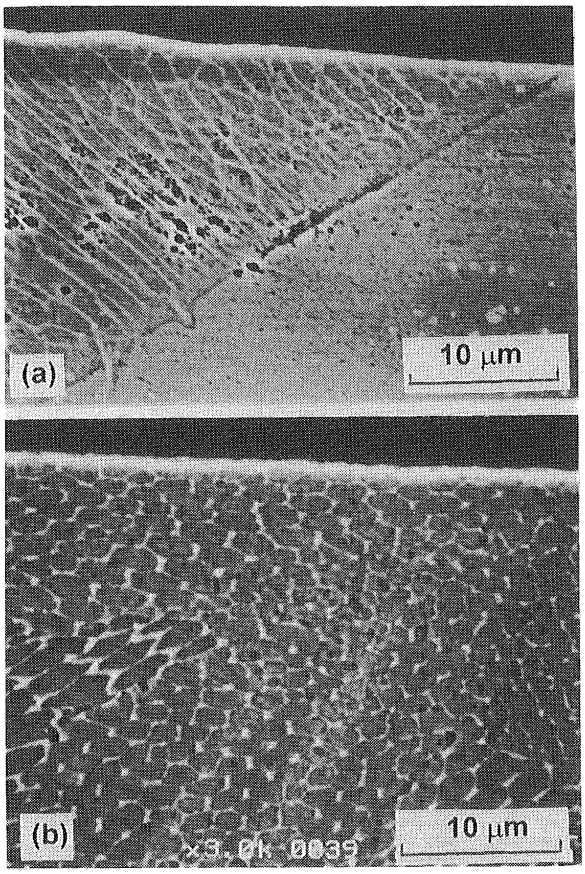

Fig.13 Cross sectional microstructures of YAG laser welds. Power 280W, Travel speed $1.3x10^{-1}$m/s

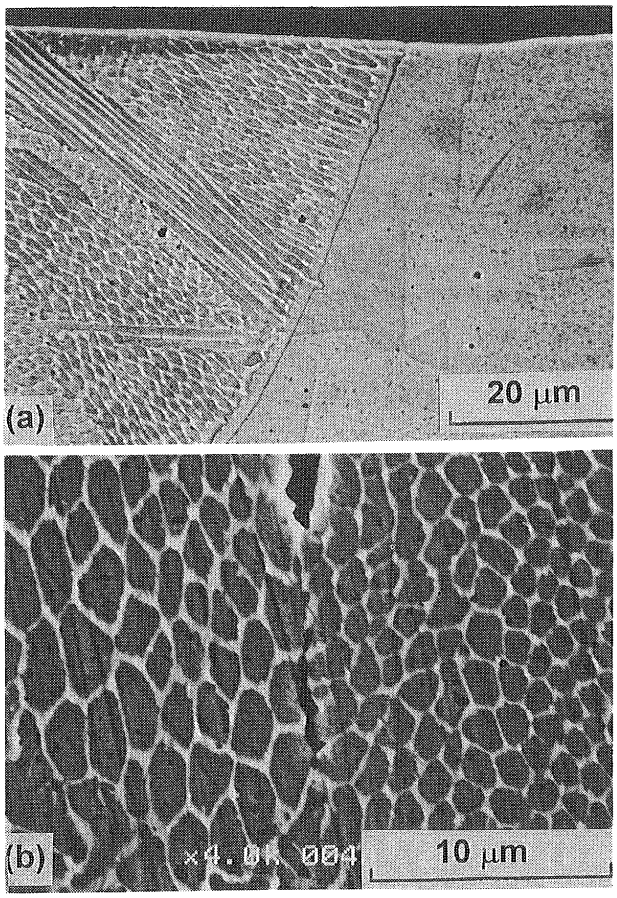

Fig.14 Cross sectional microstructures of YAG laser welds. Power 360W, Travel speed $1.3x10^{-1}$m/s

Another cross sectional area is shown in Fig.11-(b). Helium bubbles and cracks are observed at the dendrite cell boundary. The increase of weld heat input causes the growth of helium bubble and cracks.

Figure 12 shows the microstructure of the cross sectional area of the YAG Laser welds at 200W.

Large helium bubbles are observed not only in the weld metal but also in the heat affected zone. In case of the weld metal, helium bubbles and micro cracks are observed at the dendrite cell boundaries as shown in Fig.12-(a).

The helium bubbles grow with increasing weld heat input. In another cross sectional area, shown in Fig.12-(b), the cracks developed at the dendrite cell boundary and the grain boundary from the bond region to the bead surface.

Consequently, large heat input leads to cracks following the helium bubble growth.

Figure 13 indicates the microstructure of the cross sectional area, after the helium-doped SUS316L steel was laser-welded at 280W.

As shown in Fig.13-(a), large helium bubbles are present in the weld metal and at the bond region. Helium bubbles are observed in the heat affected zone. In another area shown in Fig.13-(b), helium bubbles are present at the dendrite cell boundaries and in grains.

Figure 14 shows the microstructure of the cross sectional area, as the helium-doped SUS316L steel was laser-welded at 360W

The further increase in the weld heat input has caused a decrease in the number of the helium bubbles as shown in Fig.14-(a), because the average helium concentration is lower due to the increase of the bead volume.

4. Discussion

Various mechanisms of helium bubble growth are proposed, such as grain boundary migration, recrystallization etc.

In this investigation, the helium bubble is considered to grow by absorption of thermal vacancies during the heatup period as shown in **Fig.15.**

The growth of helium bubbles is favored by conditions that promote high temperature and stress. In case of welding, the high temperature is provided by the welding arc or laser source, and stress is generated by cooling after welding.

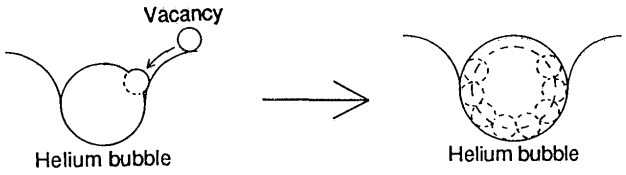

Fig.15 A growth model of helium bubble at the grain boundary by the flowing of vacancies into helium bubble

The growth kinetics of helium bubbles in the heat affected zone has been proposed by Lin, Grossbeck and Chin[3]. Their model[3] was adapted for this investigation.

The growth kinetics can be divided into the three sequential time regimes shown in **Fig.16**.

In regime II, the concentration of vacancies on a bubble surface(C_V)can be related to the equilibrium vacancy concentration(Cev) at temperature T by

$$C_V=C_{ev}\exp[-(p-2\gamma/r)V/kT \quad \text{----------(2)}$$

where V is the atomic volume, k is Boltzman's constant
p (equilibrium helium gas bubble)=$2\gamma/r$
The term C_{ev} is given by

$$C_{ev}=[\exp(\Delta S/k)\exp(-\Delta H_V/kT)]/V \quad \text{----------(3)}$$

where ΔS is the vacancy formation entropy and ΔH_V is the vacancy formation energy.
The current of vacancies into the bubble is given by

$$I = 2\pi\delta D_{gb}C_{ev}[1-\exp[-(p-2\gamma/r)V/kT]] \quad \text{---------(4)}$$

where δ is GB thickness and D_{gb} is the self-diffusion coefficient in the GB.

The volume growth rate of GB bubbles can be expressed by

$$dV/dt = I\,V \quad \text{----------(5)}$$

The growth rate of the bubble radius is given by

$$dr/dt=\delta V D_{gb}C_{ev}[1-\exp[-(p-2\gamma/r)V/kT]]/2r^2 \quad \text{-------(6)}$$

where $p=3n\gamma kT/ar^3$, ideal gas law and n_g (number of gas atoms)$=8\pi r^{2/3}kT$,
Substitution of these quantities leads to a value of 0.033 for the term $\exp[-(p-2\gamma/r)V/kT]$,

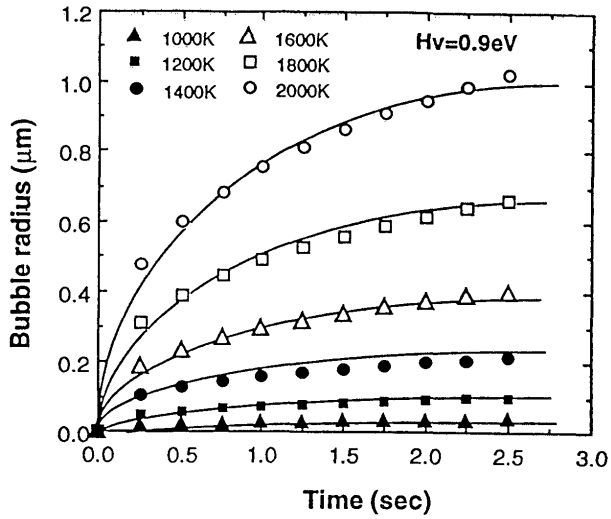

Fig.17 Helium bubble radius at grain boundary during regime II, as a function of time for different peak temperatures and ΔHv=0.9

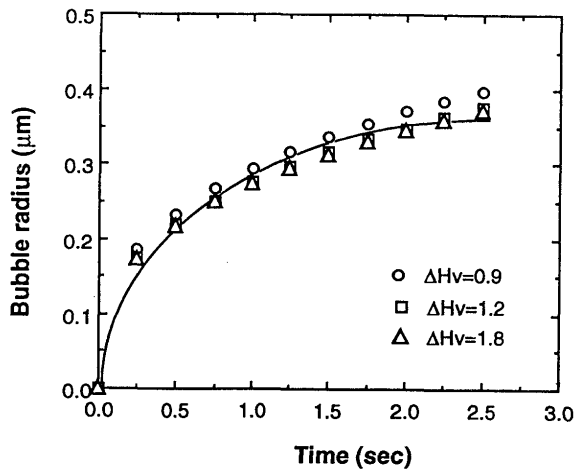

Fig.18 Helium bubble radius at grain boundary during regime II, as a function of time for three different ΔHvs and peak temperature of 1600K.

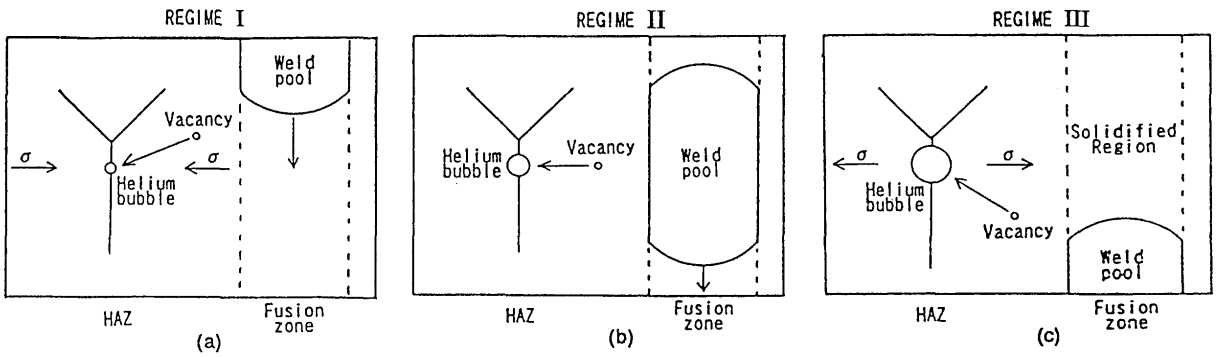

Fig.16 Schematic illustration of the growth kinetics of helium bubble at grain boundary in the HAZ during welding. (a):time regime I, (b):time regime II, (c):time regime III

which is much smaller than 1. We have from Eg.(6)

$$dr/dt = \delta V D_{gb} C_{ev}/2r^2 \quad \text{----------(7)}$$

The solution to Eq.(7) with boundary condition r=ri at t= 0.

$$r^3 - ri^3 = 3\delta V D_{gb} C_{ev} \Delta t/2 \quad \text{----------(8)}$$

where ri is the initial bubble radius in GBs and Δt is the time spent in the second regime.

Equation (8) can be used to calculate the size of bubbles in the HAZ at the end of regime II. The results were obtained by specifying

ri=1nm, ΔS=1.5k, D_{gb}=2exp(-1.65eV/kT) cm^2/s[8], $V=10^{-23}$ cm^3, and δ=0.4nm

The peak temperature-position profile in the HAZ was obtained using Adams' equation for the case of thin specimens.

One of the numerical calculations is shown in **Fig.17**. The radius of the helium bubble increases with increasing maximum temperature and holding time.

Figure 18 indicates the relation between helium bubble radius at the grain boundary and holding time at 1600K during regime II. The bubble radius is hardly affected by the ΔH_V.

The kinetics of bubble growth in regime III are essentially identical to those in regime II.

We have to consider the stress due to the thermal shrinkage during cooling after welding.

The growth rate of GB voids is approximately given by

$$dr/dt = 2\pi\delta V D_{gb}\sigma/arkT \quad \text{----------(9)}$$

The thermal stress can be expressed by

$$\delta(t) = E(t)\alpha(t)\Delta T \quad \text{----------(10)}$$

where E is 1970MPa and a is $21.4\times10^{-6}/C$[11),12)]

The instantaneous bubble size[3)] can be expressed by

$$\Delta r = 2\pi\delta V D_{gb}(r)\delta(t)\Delta t/ar(t)kT(t) \quad \text{----------(11)}$$

$D_{gb}(t)$, T(t) and a(t) are assumed to be constant within a given time interval.

During cooling, the temperature-time relationship[10)] in the HAZ is expressed theoretically by

$$T = 293+(1906/t^{1/2})\exp\{-668{,}388/[t(T_{max}-293)^2]\} \quad \text{--(12)}$$

D_{gb} (t) as a function of time can be obtained by means of Eq.13.

$$D_{gb} = 2\times10^{-4} \exp[-1.65eV/kT(t)]\ m^2/s \quad \text{------(13)}$$

Accordingly, an approximate bubble size after regime III can be obtained by iterative numerical summation of Eq.11.

The relation between helium bubble radius at a grain boundary and holding time at 1600K during regime III was claculated. As the results, the helium bubble radius increasesd with increasing holding time at 1600K.

The numerical calculations mentioned above are carried out on the basis of constant helium concentration.

In this investigation, the bead width and the penetration increased with increasing laser power and weld heat input. The increase of the weld heat input causes an increase of holding time and a decrease in the average concentration of helium.

5. Conclusion

In this research, the behavior of helium bubbles in helium doped SUS316L austenitic stainless steel weldments was investigated, by procedures in which the stainless steel was helium ion-implanted and then welded by YAG laser apparatus.

Helium ion implanting to the sample was carried out using 8MeV implantation apparatus, and the sample was doped at $2.45\times10^{19}/m^2$ and 6MeV and then $1\times10^{19}/m^2$ at 5MeV. The results are summarized as follows

(1)This technique can reproduce the helium bubble phenomena in the weld metal and in the heat-affected zone during real repair welding.

(2)When the weld heat input is low and rapid cooling conditions exit, large helium bubbles are mainly present near the region between the heat affected zone and the weld metal, and the bubbles are continuously present at the grain boundaries in the heat affected zone.

(3)Helium bubbles are present at the bond region and lead to toe cracks. An increase of weld heat input causes the growth of helium bubble and cracks.

(4)Helium bubbles are present at the dendrite cell boundaries in the weld metal, and the highest weld heat input in this study causes cracks along the dendrite cell and cracks at grain boundaries in the weld metal.

References

1)W.R. Kanne, Weld. J.,(1988),33-39
2)S. H. Goods and N. Y. C. Yang, Metall. Trans., 23A, (1992),1021-1032
3)H.T.Lin, M.L.Groobeck, B.A.Chin, Metall. Trans., 21A, (1990), 2585-2596
4)E.A.Franco-Ferreira and W.R. Kanne, Weld. J., (1992), 43-51,
5)Ion Engineering Center, Osaka, (1990)
6)J.P. Biersack and L.G. Haggmark, Nucle. Instru. Meth, 174, (1980), 257
7)J. Lindhord, M. Scharff and E. Schtt, V. Selsk, Mat. Fys. medd., No.4, (1968), 36
8)D.W. James and G.M. Leak, Phil. Mag., 12, (1965), 491-503
9)C.M.Adams, Weld. J. 37, (1958), 210s-215s
10)D.Rosenthal, Trans. ASME, 48, (1946), 849
11)D.E.Furman, trans. ASME, 188,(1950), 688-691
12)A. Wolfeden and K.Farrell, J. Nucl. Mater., 29, (1969), 133-143